12

The Hierarchies of Nonclassical Regimes for Diffusion-Limited Binary Reactions

Katja Lindenberg, Panos Argyrakis, and Raoul Kopelman

ABSTRACT Diffusion-limited binary reactions in low dimensions may lead to the spontaneous formation of spatial structures and to associated "anomalous" rate laws for the global densities of the reacting species. For example, the irreversible reactions $A + A \rightarrow 0$ and $A + B \rightarrow 0$ under "normal" circumstances are described by second-order rate laws, whereas the asymptotic rate law for the former reaction is of apparent order $(1 + 2/d)$ for dimensions $d < 2$ and for the mixed reaction it is of apparent order $(1 + 4/d)$ for $d < 4$. The slowdown implied by the higher order is a consequence of the spatial distribution of reactants and its rapid deviation from a random distribution, which is in turn a consequence of the fact that diffusion is not an effective mixing mechanism in low dimensions. The principal effect in the mixed reaction is the formation of aggregates of like particles. The spatial regions in which the density of one type of particle is overwhelmingly greater than that of the other grow in time. Since the reaction can essentially occur only at the interfaces between aggregates, and since the number of these interfaces decreases with time, the reaction slows down relative to the rate that would describe a random mixture of reactants. Note that initial spatial fluctuations in relative densities are essential for this ordering effect to occur: These fluctuations grow in size as the reaction that eliminates close opposite pairs proceeds. The particular rate law of order $(1 + 4/d)$ appropriate for an initial distribution of reactants that is completely random changes if the initial distribution is not totally random. In this chapter, we discuss the various regimes of kinetic behavior of the densities of reactants from the initial time until the asymptotic behavior is reached, and we estimate the crossover times from one regime to another. Our analysis deals with the effects of the initial conditions on this characterization. In particular, we find that initial spatial correlations limit the initial (and hence subsequent) fluctuations in the particle numbers, and hence they affect the rate laws and the underlying spatially segregated patterns. We also present numerical simulation results in one and two dimensions and analyze these results in terms of our model.

12.1 Introduction

Diffusion-limited binary reactions in low dimensions under a great variety of conditions lead to the spontaneous formation of spatial patterns and to associated "anomalous" rate laws for the global densities $\rho(t)$ of the reacting species. A vast

literature on the subject includes the references to this chapter, where many specific examples can be found. For example, the irreversible reaction $A + A \rightarrow 0$ under "normal" circumstances is described by the rate law $\dot{\rho} = -k\rho^2$ whereas [1–11] the asymptotic rate law for dimensions $d < 2$ in an infinite volume is $\dot{\rho} = -k\rho^{(1+2/d)}$. Physically, the slowdown implied by the higher exponent is a consequence of the spatial distribution of As. A random or "mixed" distribution of As has a Hertz distribution [12] of nearest neighbor distances, and this distribution in turn leads to the normal rate law. The salient characteristic of the Hertz distribution is its maximum at zero separation, indicative of the presence of many extremely close nearest neighbor pairs of reactant particles. An anomalous rate law implies a deviation from the Hertz distribution wherein there are many fewer close reactant pairs. Indeed, in dimensions lower than two, an initially random distribution quickly settles into a distribution that peaks at a finite (nonzero) nearest neighbor separation, leading to an almost crystal-like average arrangement of reactants. This nonrandom distribution arises from the fact that diffusion is not an effective mixing mechanism in low dimensions.

Another example of anomalous kinetics in low dimensions is the diffusion-limited irreversible reaction $A + B \rightarrow 0$. Under normal circumstances, the rate laws for the global densities ρ_A and ρ_B are $\dot{\rho}_A = \dot{\rho}_B = -k\rho_A\rho_B$. If $\rho_A(t = 0) = \rho_B(t = 0) \equiv \rho(t = 0)$, then the densities of the two species are equal at all times, and we can dispense with the subscripts so that once again $\dot{\rho} = -k\rho^2$. The actual asymptotic rate law in an infinite volume in dimensions $d < 4$ for an initially random distribution of reactants is instead $\dot{\rho} = -k\rho^{(1+4/d)}$. In this system, the principal cause of the anomalous behavior is the formation of aggregates of like particles. The spatial regions in which the density of one type of particle is overwhelmingly greater than that of the other grow in time (while the total density within each aggregate of course decreases with time). Since the reaction can essentially occur only at the interfaces between aggregates, and since the number of these interfaces decreases with time, the reaction slows down relative to the rate that would describe a random mixture of reactants. Again, this behavior reflects the fact that diffusion is not an effective mixing mechanism in low dimensions. Initial spatial fluctuations in relative densities can thus grow in size as the reaction that eliminates close opposite pairs proceeds.

This description of the $A + B \rightarrow 0$ reaction depends on the presence of initial spatial fluctuations in the reactant densities. The particular rate law $\dot{\rho} = -k\rho^{(1+4/d)}$ more specifically depends on an initial distribution of reactants that is completely random. A random initial distribution leads to fluctuations in the initial *local* densities so that the difference in the number of particles of type A and type B in a volume V is initially of the order of the square root of the total number of particles in that volume.

The situation of course changes with different initial fluctuations in the particle distribution. Although initial fluctuations in general tend to grow in low dimensions and hence lead to anomalous behavior in the global rate laws, the specific exponent in the rate law differs from the value $(1 + 4/d)$ appropriate for an initially random distribution, and the critical dimension for anomalous behavior in general differs

from $d = 4$.

In this chapter, we discuss the various regimes of kinetic behavior of the densities of reactants from the initial time until the asymptotic behavior is reached. The work reviewed here has to a large extent been presented elsewhere [13–15]. We characterize the various regimes and estimate the cross-over times from one regime to another. Our analysis deals with the effects of the *initial conditions* on this characterization, in particular, when the A–B pairs are initially placed in the system in a random way [13, 14] and in a spatially correlated way [13, 15]. Initial correlations limit the initial (and hence subsequent) fluctuations in the particle numbers, and hence they affect the rate laws. Indeed, we show that greater *randomness* in the initial conditions leads to *more ordered* (more segregated) asymptotic distributions and consequently to greater anomalies in the rate laws. We also present numerical simulation results in one and two dimensions and analyze these results in terms of our model.

Much of our analysis is based on the reaction-diffusion model for the local densities $\rho_A(\mathbf{r}, t)$ and $\rho_B(\mathbf{r}, t)$ [13, 16, 17]:

$$\dot{\rho}_A(\mathbf{r}, t) = D \nabla^2 \rho_A(\mathbf{r}, t) - k_l \rho_A(\mathbf{r}, t)\rho_B(\mathbf{r}, t) \tag{12.1}$$

and similarly for $\rho_B(\mathbf{r}, t)$, where k_l is the time-independent local rate coefficient and D is the diffusion coefficient for both species. It is convenient to deal instead with the difference and sum variables [13, 16, 17]

$$\gamma(\mathbf{r}, t) \equiv \frac{1}{2}[\rho_A(\mathbf{r}, t) - \rho_B(\mathbf{r}, t)], \qquad \rho(\mathbf{r}, t) \equiv \frac{1}{2}[\rho_A(\mathbf{r}, t) + \rho_B(\mathbf{r}, t)]. \tag{12.2}$$

The difference variable satisfies the linear diffusion equation

$$\dot{\gamma}(\mathbf{r}, t) = D\nabla^2\gamma(\mathbf{r}, t), \tag{12.3}$$

which can be solved exactly. The sum variable satisfies the equation obtained by summing Eq. (12.1) and its partner for $\dot{\rho}_B$:

$$\dot{\rho}(\mathbf{r}, t) = D\nabla^2\rho(\mathbf{r}, t) - k_l[\rho^2(\mathbf{r}, t) - \gamma^2(\mathbf{r}, t)]. \tag{12.4}$$

This equation can only be handled approximately.

In Sec. 12.2, we specify in detail the initial conditions to be considered and explicitly solve for the difference variable for these initial conditions. Section 12.3 describes our simulation methods. Section 12.4 deals with the analysis of the sum variable equation for the random initial distribution of reactants, the different kinetic regimes that might be observed as the densities decay from their initial distributions, and the crossover times from one sort of kinetic behavior to another. We also present simulation results and analyze them in terms of our theoretical predictions. Section 12.5 deals with the same issues for the correlated initial condition. Section 12.6 presents a brief overall summary of our results.

12.2 Initial Conditions and Difference Equation

12.2.1 Random and Correlated Initial Conditions

The initial local densities of particles are

$$\rho_A(\mathbf{r}, 0) = \sum_{j=1}^{N} \delta(\mathbf{r} - \mathbf{r}_j^A), \qquad \rho_B(\mathbf{r}, 0) = \sum_{j=1}^{N} \delta(\mathbf{r} - \mathbf{r}_j^B), \tag{12.5}$$

where $\{\mathbf{r}_j^A\}$ and $\{\mathbf{r}_j^B\}$ with $j = 1, \ldots, N$ are the initial locations. The initial distribution of particles is specified by the distribution function $p(\mathbf{r}_1^A, \ldots, \mathbf{r}_N^A; \mathbf{r}_1^B, \ldots, \mathbf{r}_N^B)$.

For random initial conditions, the locations are statistically independent [13, 14],

$$p(\mathbf{r}_1^A, \ldots, \mathbf{r}_N^A; \mathbf{r}_1^B, \ldots, \mathbf{r}_N^B) = \prod_{j=1}^{N} p(\mathbf{r}_j^A) \prod_{j=1}^{N} p(\mathbf{r}_j^B) = \frac{1}{V^{2N}}, \tag{12.6}$$

where V is the system volume and, for a random distribution of molecules,

$$p(\mathbf{r}^A) = p(\mathbf{r}^B) = \frac{1}{V}. \tag{12.7}$$

The second situation that we deal with assumes that initially *A–B pairs* are deposited at random locations (so that the single-particle distributions in Eq. (12.7) are still valid), but the members of each pair are constrained to be a distance c apart [13, 15]. Different A–B pairs may interpenetrate. The A–B distance constraint could be relaxed into a distribution around an average distance c, but if the distribution has finite moments, most of the results are similar to those found for a fixed distance. In place of Eq. (12.6), we now have the distribution function

$$p(\mathbf{r}_1^A, \ldots, \mathbf{r}_N^A; \mathbf{r}_1^B, \ldots, \mathbf{r}_N^B) = \prod_{j=1}^{N} p(\mathbf{r}_j^A, \mathbf{r}_j^B), \tag{12.8}$$

where the probability density for each A–B pair is

$$p(\mathbf{r}^A, \mathbf{r}^B) = \frac{\Gamma(d/2)}{2V\pi^{d/2}} \int d\Omega \delta(\mathbf{r}^B - \mathbf{r}^A - \mathbf{c}). \tag{12.9}$$

Here, $\mathbf{c}$ is a vector of length c and random orientation, and the integration is over these orientations, and $\Gamma(x)$ is the γ-function.

12.2.2 Solution of Difference Equations

The difference variable satisfies the linear diffusion equation, Eq. (12.3), which is easily solved (see Sec. 12.7). The quantity of interest turns out to be its mean square value $\langle \gamma^2(\mathbf{r}, t) \rangle$ (see later), where the brackets indicate an average over

the initial distribution of reactants. We find (see Sec. 12.7) for a random initial distribution of reactants,

$$\langle \gamma^2(\mathbf{r}, t)\rangle = \frac{\rho_0}{2(8\pi Dt)^{d/2}} \equiv Qt^{-d/2}. \tag{12.10}$$

Here $\rho_0 = N/V$ is the initial density of either species, and Eq. (12.10) defines the coefficient Q. For a correlated initial distribution of reactants, we find

$$\langle \gamma^2(\mathbf{r}, t)\rangle = Qt^{-d/2}\left(1 - e^{-c^2/8Dt}\right) \to Q\frac{c^2}{8D}t^{-(d+2)/2}, \tag{12.11}$$

where the last expression is valid for times $t \gg c^2/8D$.

12.2.3 Discretization

Our Monte Carlo simulations are performed on discrete lattices of lattice constant a, and the total number of lattice sites is L, so that $V = La^d$. In the continuum limit $a \to 0$ and $L \to \infty$ in such a way that V remains finite. Denoting the lattice densities by $\rho^{\text{lat}}(\boldsymbol{l}, t)$ where the index $\boldsymbol{l}$ labels the lattice sites, we have the relation $\rho \sim \rho^{\text{lat}}/a^d$. The maximum value of ρ^{lat} when multiple occupancy of a site is not allowed is thus unity. The diffusion coefficient D in the discretized problem has the value $D = 1/2$ (the distance scale implicit in the diffusion coefficient is thus different in different dimensions). For correlated initial conditions, we write the correlation distance as $c = \lambda a$, where λ is the number of lattice constants that separates a correlated pair. In our discussion of simulation results, we usually omit the superscript "lat," since the usage is clear from the context.

12.3 Method of Simulations

Simulations are performed using the conventional techniques described in our earlier papers [18–20]. Briefly, lattices of sizes up to 10^6 sites in one dimension and up to $2000 \times 2000 = 4 \times 10^6$ sites in two dimensions are generated. For random initial conditions, A and B particles are initially placed in the lattice at random but disallowing multiple occupancy of sites. Cyclic boundary conditions are utilized at the ends of the lattice. The particles then diffuse by performing independent random walks to nearest neighbor sites. Two As or two Bs are not allowed to occupy the same site. If an A and a B step onto the same site, they react, which means that they are removed from the system. Cyclic boundary conditions are employed at the ends of the lattice for the random walk as well. We monitor the particle density as a function of time for times ranging up to 10^8 steps.

For correlated initial conditions, A–B pairs are placed on the lattice so that the A particle and B particle of each pair are placed exactly λ sites apart. Here we present results only for one-dimensional simulations: First the A particle is positioned on a random site on the lattice, provided it is unoccupied. Then its B partner is placed in one of the two possible sites exactly λ sites away from the A.

The choice is again made at random. If the chosen site happens to be occupied by another particle, then the other choice is tested. If both sites at a distance λ sites away are occupied, then the pair is removed from the system, and a new effort is initiated to position the pair somewhere else. Cyclic boundary conditions are again used, so that it is possible for an A–B pair to be split at the ends of the lattice. After the initial landing of the pairs, all A and B particles perform independent random walks and carry no further memory of their counterparts. Particle densities as a function of time are again monitored for times ranging up to 10^8 steps.

Note that, contrary to the simulations, our continuum theory does not deal with excluded volume effects and hence does not disallow multiple occupancy. The unimportance of this discrepancy has been shown in detail in earlier simulations [19].

12.4 Kinetic Behavior for Random Initial Conditions

Our subsequent analysis is based primarily on the ensemble average of Eq. (12.4) over the initial distribution of reactants:

$$\langle \dot{\rho}(\mathbf{r}, t)\rangle = D\nabla^2\langle \rho(\mathbf{r}, t)\rangle - k_l[\langle \rho^2(\mathbf{r}, t)\rangle - \langle \gamma^2(\mathbf{r}, t)\rangle], \tag{12.12}$$

which makes the need for Eqs. (12.10) and (12.11) apparent. Note that the squared difference variable appears as a *source* term in the equation; the fluctuations in the difference variable thus drive the dynamics of the system. When the fluctuations in the difference variable are large, they play an important role in determining the overall dynamics. A comparison of Eqs. (12.10) and (12.11) confirms that random initial conditions allow for greater fluctuations in the difference variable than do correlated initial conditions (i.e., Eq. (12.11) decays more rapidly). This difference lies at the root of the differences in the dynamical behavior of the systems with different initial conditions.

To proceed further, one must find a way to deal with the quantity $\langle \rho^2(\mathbf{r}, t)\rangle$ and, in particular, with its relation to the global density $\rho(t) = \langle \rho(\mathbf{r}, t)\rangle$. We note that we can calculate $\langle \rho^2(\mathbf{r}, 0)\rangle$ exactly (see Sec. 12.8):

$$\langle \rho^2(\mathbf{r}, 0)\rangle = \langle \rho(\mathbf{r}, 0)\rangle^2 + \rho_{\max}\langle \rho(\mathbf{r}, 0)\rangle = \rho_0^2 + \rho_{\max}\rho_0. \tag{12.13}$$

Here, we have dropped terms of $O(N/V^2)$. The quantity $\rho_{\max}$ is the highest possible density of each reactant in the simulations with which our results will subsequently be compared: In Sec. 12.8, we deal with a discrete lattice of unit cells of volume a^d; Eq. (12.13) is obtained if one assumes that at most one molecule can be placed at each lattice site, whence $\rho_{\max} = 1/2a^d$. In a continuum model, strictly speaking, $a \to 0$ and $\rho_{\max} \to \infty$ [see Eq. (12.56)]. However, we retain it as a finite quantity to represent the effect of the finite size of the A and B molecules and the resultant excluded volume effect. Note that the second term on the right-hand side of Eq. (12.13) is greater than the first (unless $\rho_0 = \rho_{\max}$). The crux of nonclassical reaction kinetics is the departure of $\langle \rho^2(\mathbf{r}, t)\rangle$ from the relation (12.13).

To characterize this departure, we write

$$\langle \rho^2(\mathbf{r}, t)\rangle = \eta \langle \rho(\mathbf{r}, t)\rangle^2 + \mu \rho_{\max} \langle \rho(\mathbf{r}, t)\rangle, \tag{12.14}$$

which constitutes a definition of η and μ. We argue later that the variation of μ between 1 and 0 (and, less importantly, that of η between 1 and 1/2) captures all the important kinetic regimes of the $A + B \rightarrow 0$ reaction.

12.4.1 *Kinetic Regimes*

The first kinetic regime occurs *at* $t = 0$. The diffusion term in Eq. (12.12) vanishes at $t = 0$, since $\langle \rho(\mathbf{r}, 0)\rangle = \rho_0$ is independent of $\mathbf{r}$. The average $\langle \rho^2(\mathbf{r}, 0)\rangle$ is given in Eq. (12.13). Clearly, Eq. (12.10) is inappropriate for the evaluation of the initial mean square difference variable (the difficulty arises from the limits that have been taken in evaluating Eq. (12.10)). Instead, we again use the results in Sec. 12.8 to evaluate directly

$$\langle \gamma^2(\mathbf{r}, 0)\rangle = \rho_{\max} \langle \rho(\mathbf{r}, 0)\rangle = \rho_{\max} \rho_0 \tag{12.15}$$

(the infinity in Eq. (12.10) as $t \rightarrow 0$ arises from the fact that in the strict continuum limit $\rho_{\max} \rightarrow \infty$). Thus, Eqs. (12.13) and (12.15) in Eq. (12.12) at $t = 0$ yield $\langle \dot{\rho}(\mathbf{r}, t)\rangle|_{t=0} = -k_l \langle \rho(\mathbf{r}, 0)\rangle^2$, that is,

$$\dot{\rho}(t)|_{t=0} = -k_l \rho^2(0). \tag{12.16}$$

Here we have noted that $\rho(0) = \langle \rho(\mathbf{r}, 0)\rangle = \rho_0$. Equation (12.16) is precisely the *classical rate equation* for a bimolecular reaction. We note that the local rate coefficient k_l is also the rate coefficient for the global rate law in this case. Thus, very near $t = 0$ we have $\rho(t) = \rho_0/(1 + k_l \rho_0 t)$ and also $\langle \rho(\mathbf{r}, t)\rangle = \rho_0/(1 + k_l \rho_0 t)$. We must in general use this more precise form rather than $\langle \rho\rangle \sim t^{-1}$ because t is so short in this regime. Note also that this behavior could have been deduced directly from the original reaction-diffusion equation (12.1) since at $t = 0$ the diffusion term $D\nabla^2 \langle \rho_A\rangle$ vanishes because $\langle \rho_A\rangle$ is independent of $\mathbf{r}$, and the average of the product $\langle \rho_A \rho_B\rangle$ separates exactly into the product of the averages,

$$\langle \rho_A(\mathbf{r}, 0)\rho_B(\mathbf{r}, 0)\rangle = \langle \rho_A(\mathbf{r}, 0)\rangle \langle \rho_B(\mathbf{r}, 0)\rangle. \tag{12.17}$$

The analysis that leads to classical behavior at very early times is unstable to any fluctuations that lead to a deviation from the strict equality (12.17). Precisely such fluctuations are of course embodied in the driver $\langle \gamma^2(\mathbf{r}, t)\rangle$. Thus, as soon as these fluctuations destroy the equality so that

$$\langle \rho_A(\mathbf{r}, t)\rho_B(\mathbf{r}, t)\rangle \neq \langle \rho_A(\mathbf{r}, t)\rangle \langle \rho_B(\mathbf{r}, t)\rangle, \tag{12.18}$$

another kinetic behavior necessarily sets in. This is associated with the nonrandom distribution implied by Eq. (12.18). Contiguous pairs of A and B molecules react quickly, and unless diffusion can just as quickly replenish such pairs, there will be deviations from a random distribution. Although we are unable to estimate the

time t_0 at which the classical behavior ends, simulations (see following discussion) indicate that it is extremely short.

Since Eq. (12.10) is an exact result, deviations from a strictly random distribution are already built into it. In Eq. (12.14) deviations from randomness appear in the deviation of μ and η from unity. However, as long as μ is still of $O(1)$, the second term on the right-hand side of Eq. (12.14) dominates the first.

In order to balance contributions of various terms in Eq. (12.12) so as to establish the time dependence of $\langle \rho(\mathbf{r}, t) \rangle$ in the time regime where the distribution of reactants may no longer be strictly random but μ is still of $O(1)$, we explicitly substitute Eqs. (12.10) and (12.14) into Eq. (12.12):

$$\langle \dot{\rho}(\mathbf{r}, t) \rangle = D\nabla^2 \langle \rho(\mathbf{r}, t) \rangle - k_l [\eta \langle \rho(\mathbf{r}, t) \rangle^2 + \mu \rho_{\max} \langle \rho(\mathbf{r}, t) \rangle - Q t^{-d/2}]. \quad (12.19)$$

For $d = 1$ the dominant time dependence of $\langle \rho(\mathbf{r}, t) \rangle$ must be of the form

$$\langle \rho(\mathbf{r}, t) \rangle \sim \frac{Q}{\mu \rho_{\max}} t^{-1/2}. \quad (12.20)$$

The largest terms in Eq. (12.19), which are the last two terms, then balance each other. For $d \geq 2$ the dominant balance is established with the leading behavior (with perhaps logarithmic corrections in time in two dimensions) $\langle \rho(\mathbf{r}, t) \rangle \sim t^{-1}$. When $d = 2$ the dominant balance involves the diffusion term, the term linear in the density, and the last term in Eq. (12.19). In dimensions $d \geq 3$, the last term becomes unimportant.

In this "intermediate" time regime, we have thus found that the main time dependence of the mean density goes as

$$\begin{aligned} \langle \rho(\mathbf{r}, t) \rangle &\sim t^{-d/2}, \quad d \leq 2 \\ &\sim t^{-1}, \quad d > 2. \end{aligned} \quad (12.21)$$

This behavior is nonclassical in one dimension and is in fact completely analogous to the nonclassical regime of the $A+A \rightarrow 0$ and $A+A \rightarrow A$ reactions [10, 18, 21]. In those cases, the slower-than-classical decay $t^{-1/2}$ has been well documented to arise from the "depletion zone" that forms around each surviving reactant after the initially very close pairs have quickly reacted [1, 11]. Diffusion in one dimension is known to be an ineffective mechanism toward refilling the depletion zone [18, 22, 23]. The same happens here in the $A + B \rightarrow 0$ reaction. After the rapid initial reaction of very nearby A–B pairs (classical regime), each surviving A and B is surrounded by a region relatively poor in the other species (depletion zone) [18, 24, 25]. In our analysis of the dominant balances of terms in Eq. (12.19) in one dimension, the diffusion term was indeed a higher-order contribution, while the dominant contribution came from the species fluctuational contribution. The logarithmic corrections to classical behavior $\langle \rho(\mathbf{r}, t) \rangle \sim t^{-1}$ in two dimensions are well documented in the $A + A$ problems [18, 20, 23, 25–28]. In dimensions $d \geq 3$, the behavior is dominated by the classical contributions. Diffusion is now effective in countering any depletion around reactants, and species density fluctuations play only a higher-order role.

After a sufficiently long time has elapsed, it is well known [1, 2, 18, 24, 29–31] that the system evolves toward macroscopic segregation and that $\langle \rho(\mathbf{r}, t) \rangle \sim t^{-d/4}$ for $d < 4$. This behavior is captured if we set $\mu = O(\langle \rho \rangle / \rho_{\max})$ and $\eta = 1/2$ in Eq. (12.14) (see following discussion). The choice $\eta = 1/2$ implies a complete segregation of species, i.e., that $\langle \rho_A(\mathbf{r}, t) \rho_B(\mathbf{r}, t) \rangle = 0$. This choice is not crucial to the term balancing arguments. More important is the choice of μ. One might naively assume that the $t^{-d/4}$ behavior is mainly due to the macroscopic segregation and that the spatial distribution of molecules within each aggregate is of lesser importance. This is not the case. Indeed, were we to assume an essentially random distribution within each aggregate, we would set $\mu \approx 1$, and we would be back to the previous analysis, with the result that $\langle \rho(\mathbf{r}, t) \rangle \sim t^{-d/2}$ for $d \leq 2$. In reality, the formation of macroscopic aggregates is accompanied by a nonrandom (clumped up) distribution within each aggregate [18, 24]. Hence the choice $\mu \ll 1$. We will see that setting $\mu = O(\langle \rho \rangle / \rho_{\max})$ captures the proper behavior. Thus, in this regime, in place of Eq. (12.19) we now analyze the balances implicit in

$$\langle \dot{\rho}(\mathbf{r}, t) \rangle = D \nabla^2 \langle \rho(\mathbf{r}, t) \rangle - k_l [\alpha \langle \rho(\mathbf{r}, t) \rangle^2 - Q t^{-d/2}], \tag{12.22}$$

where $\alpha = O(1)$ [13, 17].

For $d \leq 4$ the dominant balance must occur inside the square brackets, whence

$$\langle \rho(\mathbf{r}, t) \rangle \sim \left(\frac{Q}{\alpha} \right)^{1/2} t^{-d/4}. \tag{12.23}$$

For $d > 4$ a balance occurs if $\langle \rho(\mathbf{r}, t) \rangle \sim B t^{-1}$ (classical behavior). This balance does not involve the $\langle \gamma^2 \rangle \sim t^{-d/2}$ term.

Any simulation with which we wish to compare our analysis necessarily takes place in a finite volume. At sufficiently long times, finite volume effects will therefore affect the results of such simulations. It is well known that finite volume effects eventually cause an exponential decay of the density:

$$\langle \rho(\mathbf{r}, t) \rangle \sim e^{-\chi t}, \tag{12.24}$$

where χ is a constant inversely proportional to the square of the linear size L of the system, $\chi \sim L^{-2}$. This behavior is expected to take over when the size of each aggregate is of the order of the size of the system, or, if the initial density is too small to lead to segregation before finite size effects set in, when the average distance between particles is of the order of the size of the system.

12.4.2 Crossovers

The "major" crossover time t_s and average crossover density ρ_s for $d \leq 4$ occur when the $t^{-d/4}$ segregation behavior sets in. For $d \leq 2$ this occurs from the depletion zone, while for $d > 2$ it occurs directly from the classical regime. In either case, this onset is determined by the rough balance of all three terms in the square brackets in Eq. (12.19). We recall that well before this onset $\mu \sim O(1)$,

while in the segregation regime, $\mu \sim O(\langle\rho\rangle/\rho_{\max})$. At crossover, we set $\eta = 1/2$, assuming substantial segregation to have begun. We write the crossover density as a fraction of the initial density,

$$\rho_s \sim f_d \rho_o, \tag{12.25}$$

where f_d is a dimension-dependent fraction assumed to be of $O(1)$ and independent of the initial density. The balance of the first two terms in the square brackets in Eq. (12.19) then yields $\mu_s \sim f_d \rho_o / 2\rho_{\max}$. The balance of the first and third terms, $\rho_s^2/2 \sim Q t_s^{-d/2} \sim f_d^2 \rho_o^2/2$, yields for the crossover time with Q given by Eq. (12.10)

$$t_s \sim \frac{1}{8\pi D \rho_o^{2/d} f_d^{4/d}}. \tag{12.26}$$

Equations (12.26) and (12.25) are the main results of this section to be tested against numerical simulations. The value of f_d must be determined from the simulations. If our assumption that f_d is independent of ρ_o is correct, then $t_s \rho_o^{2/d}$ should be independent of the initial density ρ_o. Likewise, the ratio of the crossover density to the initial density, ρ_s/ρ_o, should be independent of ρ_o.

For $d = 1$ there is an additional crossover at very early times from the classical $(\rho_o/(1 + k_l t \rho_o))$ to the depletion zone $t^{-1/2}$ behavior. We do not have a quantitative estimate of this crossover time. It may be similar to that for the $A + A \to A$ reaction, solved exactly by Doering and Ben-Avraham [21].

Finally, at long times, the finite size of the system causes an exponential decay of the densities. When the initial density is high enough for there to be a segregation regime, the finite size effects set in when the aggregates of like molecules are of the order of the size of the system. For $d = 1$ and $d = 2$, it is known [2, 25, 31], that the linear size of the aggregates on the average grows with time as $a_d(Dt)^{1/2}$. Here a_d is a dimension-dependent constant of proportionality, which, based on the work of Leyvraz and Redner [25], appears to be approximately 4 in one dimension. There is actually a distribution of aggregates around this average that is skewed toward large aggregates. Finite size effects are thus expected to set in at a time t_f such that the average linear size of the aggregates is some fraction $g_d \sim O(1)$ of the linear size L of the system, $a_d(Dt_f)^{1/2} \sim g_d L$; i.e.,

$$t_f \sim g_d^2 \frac{L^2}{a_d^2 D}. \tag{12.27}$$

Here g_d, a dimension-dependent fraction expected to be independent of the initial density, is to be determined from simulations.

On the other hand, if the initial density is low, then segregation may never be observed, because finite size effects set in when the average distance between particles is of the order of the size of the system; i.e., when

$$\frac{1}{\rho_f} \sim L^d. \tag{12.28}$$

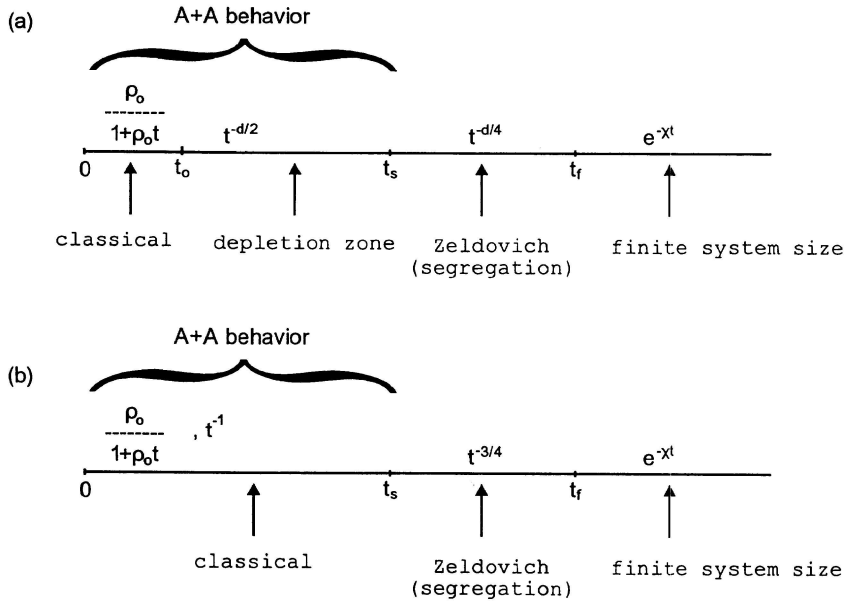

FIGURE 12.1. Possible time progression of kinetic behaviors discussed in the text for a random initial condition. (a) $d \leq 2$; (b) $d = 3$.

The associated time t_f depends on whether the density ρ_f is achieved in the depletion zone regime or in the classical regime and must be extracted accordingly.

Figure 12.1 summarizes a possible progression of kinetic behaviors as discussed earlier. In Fig. 12.1, we have assumed that $t_f \gg t_s$. This need not be the case: As the system size decreases, t_f sets in earlier and earlier.

12.4.3 Comparison With Monte Carlo Simulations

Figure 12.2 shows our Monte Carlo simulation results for the reactant density as a function of time for random initial conditions in one-dimensional lattices of various sizes L. The initial density in all cases is $\rho_0 = 0.2$ for each species. Here and later, densities are in units of particles per site. The initial slope in all cases is seen to be the same as that of the $A + A$ problem; indeed, the initial slope in Fig 12.2 overlaps that of a direct $A + A$ simulation. In turn, $A + A$ kinetics is initially classical (slope 1 in Fig. 12.2) but very quickly crosses over to the $t^{-1/2}$ behavior characteristic of the depletion zone (slope 1/2 in Fig. 12.2). We find that the "average slope" over the first 10 steps is 0.55. At very long times, the largest lattices show the Zeldovich behavior. Indeed, for the largest lattice we find an average slope of 0.249 over the last decade of the simulation. The crossover time from the $A + A$ depletion zone

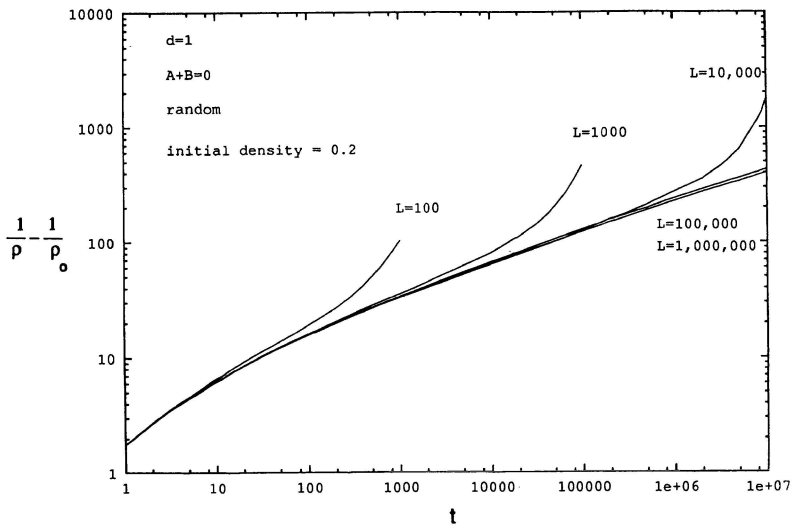

FIGURE 12.2. $\langle\rho\rangle^{-1} - \rho_0^{-1}$ vs. t for lattices of various sizes L in one dimension with a random initial condition. The initial density of each species in number per lattice site is $\rho_0 = 0.2$ in all cases.

behavior to the Zeldovich behavior is discussed later and found to be $t_s \sim 10^2$. The smaller lattice simulations show the "peel off" due to finite lattice size effects. Each of the simulations for $L = 100$, 1000, and 10,000 was cut off when only a single particle of each kind was left on the average. For $L = 100$ we find that finite size effects begin to set in when $t = t_f \sim 20$. According to Eq. (12.27), the average size of the aggregates is approximately $g_1 L \sim 4(Dt_f)^{1/2} \sim 13$; i.e., $g_1 = 0.13$. Thus, each aggregate of each species is on the average larger than 1/10 of the size of the system (which of course must contain at least two aggregates). There is a substantial probability of even larger aggregates [25].

Since we assume that the fraction g_d is independent of L, we can use the value of g_1 obtained earlier to predict the crossover times t_f for the other lattices. We find that $t_f \sim 2 \times 10^3$ for $L = 1000$ and $t_f \sim 2 \times 10^5$ for $L = 10,000$. Both of these are consistent with the simulation results. To emphasize this point, in Fig. 12.3 we have replotted the results of Fig. 12.2 as a function of the *scaled* time t/L^2. On this scale, the finite size effects for all the finite lattices begin to appear at approximately $t_f/L^2 \sim 2 \times 10^{-3}$. Figure 12.3 makes evident the scaling relation $t_f \sim L^2$.

Note that although the larger systems contain larger aggregates when finite system size effects set in, the number of particles per aggregate at that point is smaller in the larger lattices, since more time has gone by and therefore the total density has had an opportunity to decrease further than in the smaller lattices.

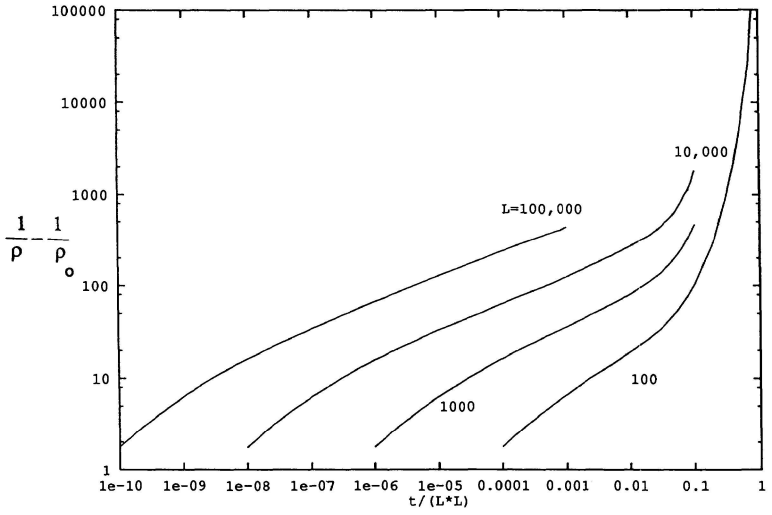

FIGURE 12.3. $\langle \rho \rangle^{-1} - \rho_0^{-1}$ vs. scaled time t/L^2 for the same cases as in Fig. 12.2.

Figure 12.4 shows our Monte Carlo simulation results for the reactant density as a function of scaled time for random initial conditions in a one-dimensional lattice for various initial densities ρ_0. Straight lines have been drawn to aid in the visualization of the crossover times t_s from one kinetic behavior ($t^{-1/2}$) to another ($t^{-1/4}$). The crossover time t_s is of course not sharply defined, and therefore these lines are not to be taken too literally. The lowest densities do not reach the crossover within the time regime shown. Note also that finite lattice size effects are not apparent in the time regimes shown in this figure. The product $t_s\rho_0^2$ is fairly insensitive to the initial condition, as predicted in Eq. (12.26). The observation that $t_s\rho_0^2 = O(10^0) - O(10^1)$ leads to $f_d \sim 0.3 - 0.5$. This in turn leads to values of $\rho_s \sim f_d\rho_0$ that are indeed consistent with the crossover densities in Figure 12.4.

Figure 12.5 shows the Monte Carlo results for the reactant density vs. time for random initial conditions in two-dimensional lattices of various sizes (cf. Fig. 12.2). Again, the initial density in all cases is $\rho_0 = 0.2$ for each species. The initial slope is consistent with the $A + A$ behavior of unity within logarithmic corrections. The average slope over the first ten steps is 0.78. At long times, the largest lattices show Zeldovich behavior: We find a slope of 0.53 in the time domain $10^4 - 10^5$ for the largest lattice; the crossover time to this behavior occurs at $t_s \sim 250$ (see later).

For $L = 60$ we find that finite size effects begin to set in when $t = t_f \sim 150$. We do not have explicit information about the proportionality constant a_2 in Eq. (12.27), so we can only determine the ratio g_2/a_2 from this information, $g_2/a_2 \sim$

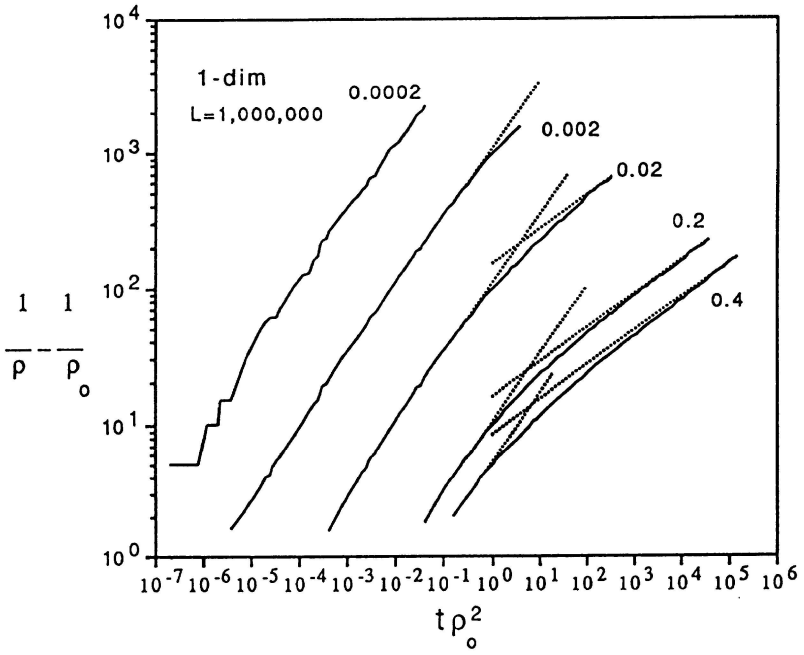

FIGURE 12.4. $\langle\rho\rangle^{-1} - \rho_o^{-1}$ vs. $t\rho_o^2$ in one dimension with a random initial condition for the various initial densities indicated. Simulations are on one-dimensional lattices of one million sites. The initial densities are in number per lattice site.

0.14. If $a_2 \sim a_1 = 4$, this would give $g_2 \sim 0.6$, but we have no basis for this particular choice. However, since we assume that both a_d and g_d are independent of L, we can use this ratio to predict the crossover times t_f for the other lattices according to the relation $t_f \sim 0.041\ L^2$. We thus find $t_f \sim 1660$ for $L = 200$, $t_f \sim 1.5 \times 10^4$ for $L = 600$, and $t_f \sim 1.7 \times 10^5$ for $L = 2000$. These are all consistent with the simulation results. Again, to emphasize this point, in Fig. 12.6 we have replotted the results of Fig. 12.5 as a function of the *scaled* time t/L^2. On this scale, the finite size effects for all the finite lattices begin to appear at approximately $t_f/L^2 \sim 4 \times 10^{-2}$. Figure 12.6 again makes evident the scaling relation $t_f \sim L^2$.

Figure 12.7 shows our Monte Carlo results for the reactant density as a function of scaled time for random initial conditions in a two-dimensional lattice for various initial densities. The crossover from the early time t^{-1} behavior to the $t^{-1/2}$ Zeldovich behavior has been noted at the higher initial densities. Again, the insensitivity of $t_s\rho_o$ to the initial density as predicted in Eq. (12.26) is evident. With the value $f_d \sim 0.03$ read from these results, one can see that the prediction $\rho_s \sim f_d\rho_o$ is again excellent (i.e., f_d is independent of ρ_o). At long times, the crossover to

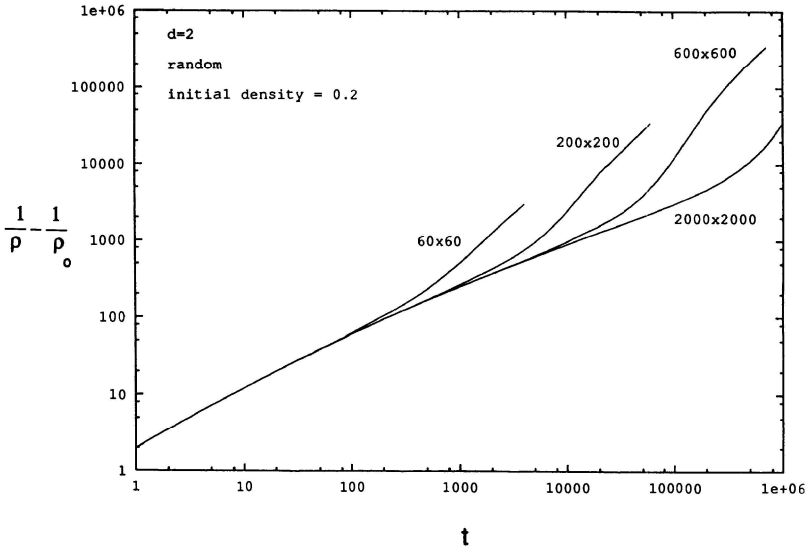

FIGURE 12.5. $\langle\rho\rangle^{-1} - \rho_0^{-1}$ vs. t for two-dimensional lattices of various sizes $L \times L$ with a random initial condition. The initial density of each species is $\rho_0 = 0.2$ in all cases.

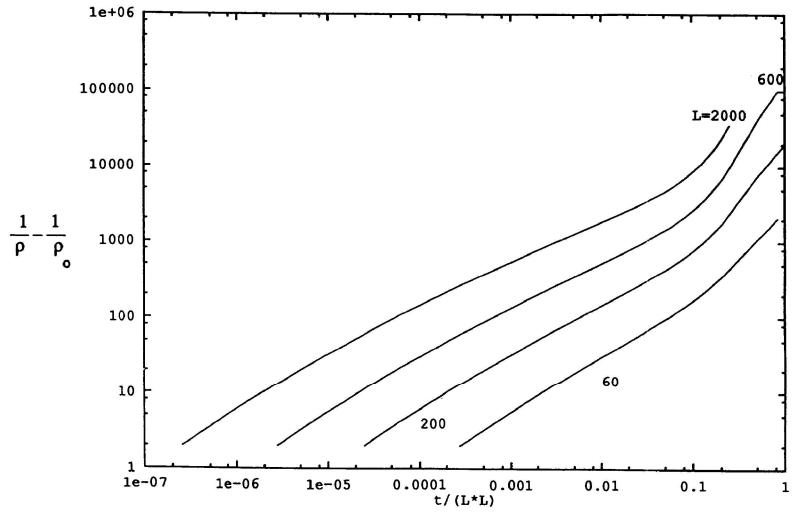

FIGURE 12.6. $\langle\rho\rangle^{-1} - \rho_0^{-1}$ vs. scaled time t/L^2 for the same cases as in Fig. 12.5.

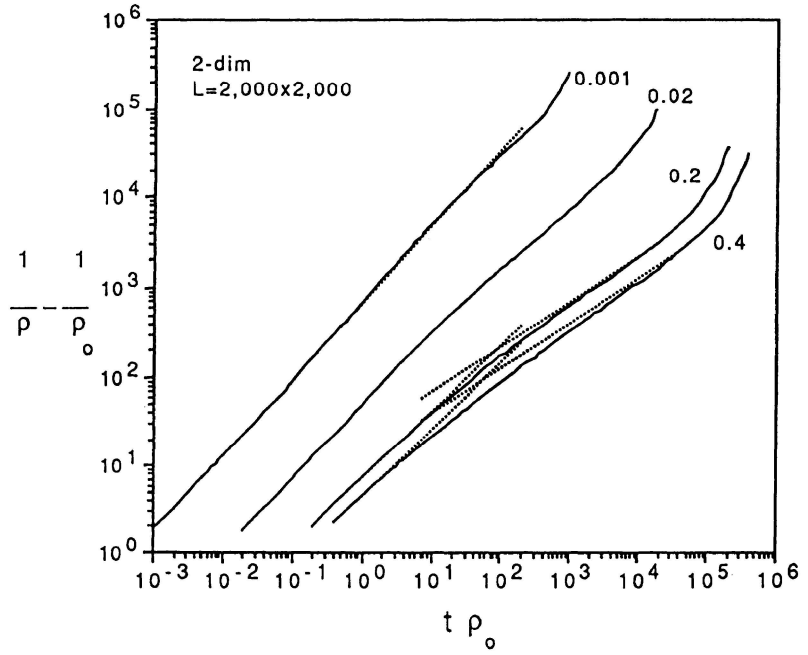

FIGURE 12.7. $\langle\rho\rangle^{-1} - \rho_0^{-1}$ vs. $t\rho_0$ in two dimensions with a random initial condition for the various initial densities indicated. Simulations are on two-dimensional lattices of 2000×2000 sites.

finite size effects is apparent in the upturn of all the curves.

12.5 Kinetic Behavior for Correlated Initial Conditions

The continuum limit implicit in a reaction-diffusion equation places certain constraints on parameter values and variables. One of these is that the correlation distance c must be sufficiently large for there to be many particles between correlated pairs; i.e., we must have $\langle\rho(\mathbf{r}, t)\rangle c^d \gg 1$. This condition can at best hold only up to some time t; once $\langle\rho(\mathbf{r}, t)\rangle$ becomes sufficiently small, the condition is necessarily violated. Nevertheless, we can still argue heuristically about some features of the behavior of the system even at very low densities.

We begin again with the ensemble-averaged equation (12.2). For the initially correlated distribution of reactants, we again obtain Eq. (12.13) (restricting ourselves to $\lambda \neq 0$). Therefore, we again write Eq. (12.14) as a way to characterize the departure of $\langle\rho^2(\mathbf{r}, t)\rangle$ from the initial form.

Our earlier analysis of the random initial condition case was explicitly or im-

plicitly based on the appearance of a number of length scales whose interplay determines the way in which the system evolves. One of these is the distance between nearest neighboring particles; the second is the linear size of an aggregate of like particles, and the third is the size of the system. Here, a fourth length scale appears, namely, the distance c initially separating a correlated A–B pair. This additional length leads to a rich variety of new behavior determined by its size relative to the other scales.

12.5.1 Kinetic Regimes and Crossovers

We assume that the continuum condition holds at least initially, i.e., $\rho_0 c^d \gg 1$, and will later comment on the behavior of the system when this is not the case. The $t = 0$ analysis presented in Sec. 12.4.1 is still valid and leads to classical behavior until the instabilities that lead to Eq. (12.18) set in. This is not surprising; at very early times, reacting pairs of particles are not correlated pairs since the latter are still too far apart. Instead, reactions involve uncorrelated partners, and the dynamics is therefore indistinguishable from the random situation.

As time proceeds, the principal new behavior here arises from the change in $\langle \gamma^2(\mathbf{r}, t)\rangle$ (see Eq. (12.11)), which now in place of Eq. (12.19) leads to

$$\langle \dot{\rho}(\mathbf{r}, t)\rangle = D\nabla^2\langle \rho(\mathbf{r}, t)\rangle - k_l[\eta\langle \rho(\mathbf{r}, t)\rangle^2 + \mu\rho_{\max}\langle \rho(\mathbf{r}, t)\rangle - Qt^{-d/2}\left(1 - e^{-c^2/8Dt}\right)]. \tag{12.29}$$

The dominant balances now depend not only on η and μ but also on the relative importance of the exponential contribution to the last term. The exponential becomes important at times $t \sim t_c$, where t_c is proportional to the time that it takes on the average for a particle to cover a distance c,

$$t_c \equiv c^2/8D. \tag{12.30}$$

At times greater than t_c, correlated particles have had an opportunity to meet one another; at times prior to t_c, correlated particles "do not know" of one another's existence, and the system should therefore behave as with a random initial condition. This is indeed the case. The differences between the random and correlated systems only set in beyond time t_c, and the entire further analysis depends on where this time falls in relation to the other characteristic times of the system. This is simply another way of saying that the subsequent behavior depends on the relation of the length scale c to the other characteristic length scales.

If t_c is greater than t_0, then the transition to depletion zone behavior will again occur at time t_0. The subsequent behavior of the system depends on the relative magnitudes of the time t_s introduced in Eq. (12.26) and the time t_c. Recall that t_s marks the beginning of the aggregation process in the random initial condition case and the consequent slowing down of the reaction. If t_s is smaller than t_c, then the evolution of the correlated system continues as that of the random system, and segregation begins to set in before the correlation length is felt by associated

partners. If, on the other hand, $t_s \gg t_c$, then the correlation effects are felt before segregation sets in, segregation does not occur, and the behavior is quite different. We discuss these two cases separately.

Dynamics with Segregation. Consider first the case $t_s \ll t_c$. With the explicit expressions in Eqs. (12.26) and (12.30), the condition $t_s \ll t_c$ can be translated to the statement

$$c^d \rho_0 \gg \frac{1}{\pi^{d/2} f_d^2}. \tag{12.31}$$

In one dimension, our simulation results led to $f_d \sim 0.3 - 0.5$, so that Eq. (12.31) requires that $c\rho_0 \gg 6$: If this condition is satisfied, then segregation sets in at time t_s as in the random initial condition case. In two dimensions, we found $f_d \sim 0.03$, so that segregation sets in at time t_s, provided that $c^2\rho_0 \gg 350$. Note that with condition (12.31) both in one and two dimensions, the density of the system at time t_s still satisfies the condition for the continuum approximation to be applicable; i.e., $c^d \rho_s \sim c^d f_d \rho_0 \gg 1$. This is consistent with the notion that segregation implies the existence of many particles separating correlated partners. Note that in this segregation regime, as time and the reaction proceed, the system density decreases while the number of particles in each aggregate of like particles increases relative to the total number of particles.

Segregation continues as with a random initial condition until time t_c: At this time the exponential contribution to the last term in Eq. (12.29) becomes important, and the balance of terms changes. Note that the average density ρ_c at this time is still sufficiently high for the continuum approximation to be valid. An estimate of ρ_c can be obtained from the relation $\rho_c \sim (t_c/t_s)^{-d/4}\rho_s$, which leads to the expression

$$c^d \rho_c \sim \frac{(c^d \rho_0)^{1/2}}{\pi^{d/4}}. \tag{12.32}$$

With $c^d \rho_0 \gg 1$, we then satisfy the continuum condition for $c^d \rho_c$ as well.

At and beyond times $t \sim t_c$, the exponent in Eq. (12.29) can be expanded and Eq. (12.29) can be rewritten as

$$\langle \dot{\rho}(\mathbf{r}, t)\rangle = D\nabla^2\langle \rho(\mathbf{r}, t)\rangle - k_l[\eta\langle \rho(\mathbf{r}, t)\rangle^2 + \mu\rho_{\max}\langle \rho(\mathbf{r}, t)\rangle - \frac{Qc^2}{8D}t^{-(d+2)/2}]. \tag{12.33}$$

At time t_c, the system is still segregated. Since in general the size of an aggregate at time t is of the order of the region covered by a random walker in time t (at least in dimensions $d \leq 2$, where random walks are compact), the average linear dimension of the aggregates of like particles at t_c is $\sim c$. The coefficient η in Eq. (12.33) is of $O(1)$, while $\mu \sim O(0)$, and the dominant balance then immediately leads to

$$\begin{aligned} \langle \rho(\mathbf{r}, t)\rangle &\sim t^{-(d+2)/4} \qquad \text{for } d \leq 2, \\ &\sim t^{-1} \qquad \text{for } d > 2. \end{aligned} \tag{12.34}$$

The decay of the density in Eq. (12.34) not only is faster than that of the segregation regime but, for $d \leq 2$, indeed, is even faster than in the $A+A$ depletion zone regime! This behavior comes about because the correlated initial condition places a limit of order c on the size of a segregated aggregate. The initial correlations suppress fluctuations in relative densities of A and B particles necessary for the growth of the segregation pattern to continue beyond that. Indeed, as time increases beyond t_c and the overall density of particles continues to decrease due to the reaction, so does the number of like particles in an aggregate relative to the total number of particles. As a consequence, the relative number of A–B interfaces at which the reaction can take place increases. This "shrinkage" of aggregates leads to the rapid decay in Eq. (12.34).

Eventually, a configuration is reached where each A particle is essentially surrounded by Bs and vice versa; the aggregates have now "shrunk" to essentially single particles. This occurs at a time that we call t_{es} (the subscript stands for "end of shrinkage") at an average density ρ_{es} determined from the fact that the only surviving particles in the aggregates of size c are those in the center of the aggregates, i.e., such that $c^d \rho_{es} \sim O(1)$. These surviving particles are at a distance of order c apart. It is important to note that in general A–B pairs that are now a distance c apart are *not* originally correlated partners, since chances are that the correlation partner of any given particle has already reacted. The configuration at this point is only indirectly reflective of but certainly due to the original correlations. The time t_{es} can be estimated from the relation $\rho_{es} \sim (t_c/t_{es})^{-(d+2)/2}\rho_c$. With Eqs. (12.30) and (12.32), this estimate leads to $t_{es}/t_c \sim (c^d \rho_0/\pi^{d/2})^{1/(d+2)}$. For $d = 1$ this reduces to

$$\left(\frac{t_{es}}{t_c}\right) \sim \left(\frac{c\rho_0}{\sqrt{\pi}}\right)^{1/3}, \tag{12.35}$$

a form that is useful for our later analysis. Note that the times t_{es} and t_c become ever closer with decreasing c and decreasing ρ_0. Therefore, the aggregate shrinkage regime can be seen more clearly with larger values of c (for given ρ_0). This in turn requires that the simulation be carried out to very long times.

At time t_{es} the continuum approximation has ceased to be valid, so that further arguments must be made heuristically. A–B pairs are now narrowly distributed around a distance c, so after a time narrowly distributed around $\sim c^2/2D$ they will meet and react. Until this happens, the density does not change much. Thus, at a time of order

$$t_{sb} \sim t_{es} + c^2/2D \sim t_{es} + t_c \tag{12.36}$$

we expect a sharp increase in the reaction rate. We call this a *slow burst* (a further discussion of bursts and slow bursts follows). Following the slow burst, the system returns to the uncorrelated depletion zone $A + A$ behavior ($t^{-d/2}$) at a time t_r, a behavior that may be overshadowed by the onset at t_f of finite system size effects. Finite size effects lead to exponential decay of the density when $\langle\rho\rangle \sim 1/L^d$.

Figure 12.8 summarizes the progression of kinetic behaviors discussed above.

Dynamics without segregation. Next, consider the situation where the correlation

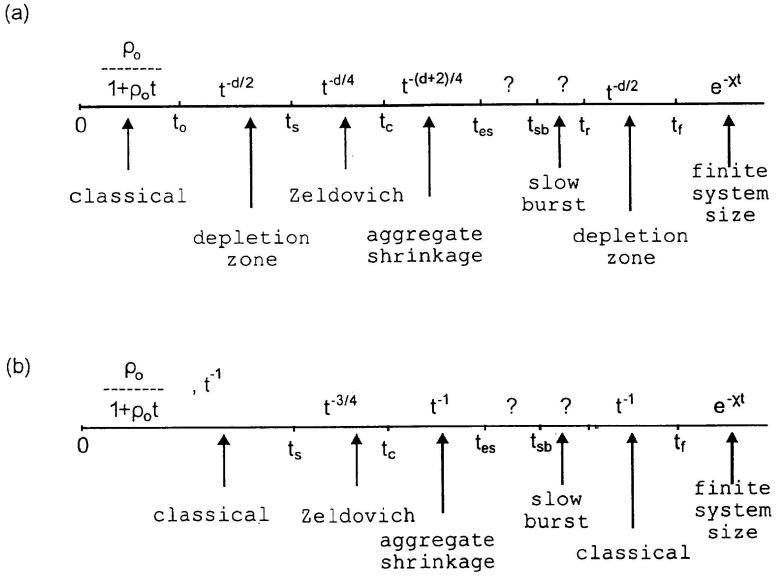

FIGURE 12.8. Possible time progressions of kinetic behaviors for a correlated initial condition when the initial particle density is sufficiently high for there to be a segregation regime. (a) $d \leq 2$; (b) $d = 3$.

distance is sufficiently short that correlation effects set in before segregation can occur; that is, $t_c < t_s$. In this case, even if initially $c^d \rho_0 > 1$, $c^d \langle \rho(\mathbf{r}, t) \rangle$ becomes of $O(1)$ at time t_c while the system is still in the $A + A$ depletion regime or perhaps even in the classical behavior mode. Our arguments in this regime are therefore heuristic, since the continuum approximation is no longer valid. In this case there should be no distinction between the $A + B$ and $A + A$ problems over the entire time regime; that is, initially tightly correlated $A + A$'s should evolve in exactly the same way as initially tightly correlated $A + B$'s. Figure 12.9 is a typical simulation in this regime that shows the reactant density for both reactions. In this particular one-dimensional simulation, $c\rho_0 = 2$. As we will see later, when the initial pairs are even more tightly correlated, the evolution of the two reactions is even more parallel.

Consider first the very low initial density case, $c^d \rho_0 < 1$. An important behavior-determining feature in this situation is the fact that, with the exception of a few uncorrelated pairs that were initially closer than distance c and that may therefore react before time t_c, originally correlated pairs are now able to react because they have an opportunity to encounter one another before either partner has reacted with another molecule. This fact, coupled with the fact that correlated pairs started out at exactly a distance c apart, means that at times very narrowly distributed around

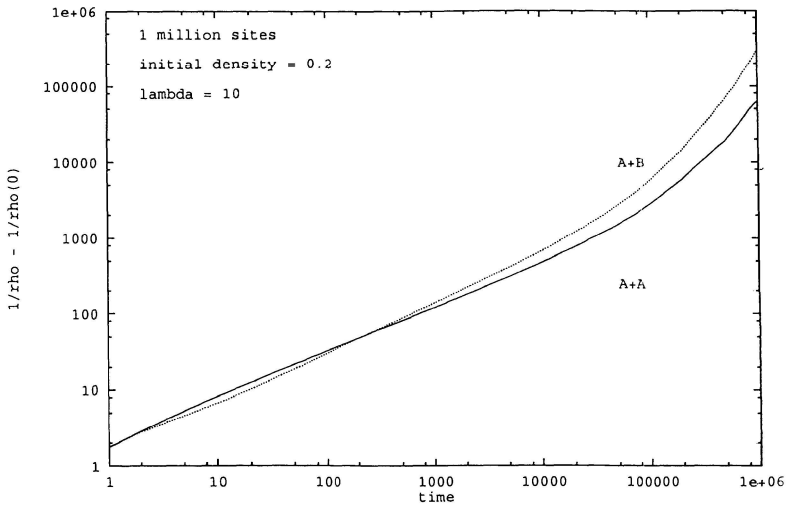

FIGURE 12.9. $\langle\rho\rangle^{-1} - \rho_0^{-1}$ vs. t in one dimension with a fairly tightly correlated initial condition for the initial density $\rho_0 = 0.2$. The evolution for the two reactions is very similar.

t_c many pairs suddenly encounter one another, and the reaction rate suddenly experiences a sharp (short-lived) burst. We thus expect the density to experience a sharp decrease at times $t \sim t_c$. Note that this burst due to the reaction of correlated partners is not observed in the high initial density case, but a remnant of this effect is observed (the slow burst). Once the burst is over because most of the initially correlated pairs have reacted with one another (time t_r), the situation reverts back to that of the uncorrelated $A + A$ problem, since each remaining particle is essentially surrounded by uncorrelated particles of the opposite kind. The system thus never reaches the Zeldovich regime, and the asymptotic behavior for an infinite system is $t^{-d/2}$ ($d \leq 2$), or t^{-1} ($d \geq 3$). The return to the depletion zone behavior may again be overshadowed by finite size effects.

Next consider the case $c^d\rho_0 > 1$ (but $c^d\rho_0$ not sufficiently large for segregation to occur). In this case, there is still a burst that sets in at around t_c, albeit a slow one (reflective of the initial interpenetration of correlated pairs). This slow burst is consistently observed for *both* $A + A \rightarrow$ and $A + B \rightarrow$ reactions.

Figure 12.10 summarizes the progression of kinetic behaviors discussed above.

12.5.2 Comparison With Monte Carlo Simulations

Figure 12.11 shows the Monte Carlo simulation results for one-dimensional lattices of one million sites for various correlated initial conditions. The initial density in

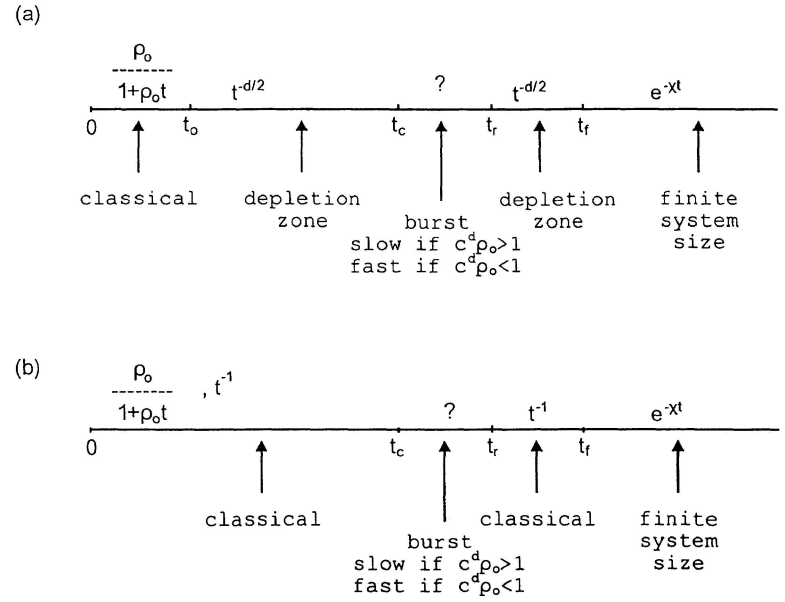

FIGURE 12.10. Possible progressions of kinetic behaviors for a correlated initial condition when the initial particle density is not sufficiently high for there to be a segregation regime. (a) $d \leq 2$; (b) $d = 3$.

all cases is 0.2 particles of each species per lattice site. The discrete correlation distance λ is indicated on each curve. The "random" curve corresponds to the random initial condition and is the same as the $L = 1{,}000{,}000$ curve in Fig. 12.2.

Consider the λ =10,000 curve in Fig. 12.11a, for which $\rho_0\lambda = 2000 \gg 6$. The expected kinetic progression is as shown in Fig. 12.8a. The time t_s should occur in the same region as for the random initial condition, since t_s is independent of the correlation distance. Earlier, we found that for $\rho_0 = 0.2$, $t_s \sim 10^2$. The independence of t_s from λ is indeed observed in Fig. 12.11a; the two curves are superimposed for times that are much longer than t_s. The faster decay of the λ = 10,000 density is expected to set in at about $t_c = \lambda^2/8D = (10{,}000)^2/4 = 2.5 \times 10^7$. This is consistent with the observed behavior. We find that in the range 2×10^7 to 10^8 the average slope of the curve is 0.77, that is, close to the predicted 3/4. The reactant density predicted from Eq. (12.32) at t_c is $\rho_c \sim 3 \times 10^{-3}$, which is consistent with the density obtained from Fig. 12.11a at t_c. The crossover time t_{sb} into the slow burst regime is predicted at about 10^8 (see Eq. (12.35)), that is, beyond our time scale. However, we do see the beginning of a sharp increase in the reaction rate, perhaps indicative of the expected slow burst.

Next consider the λ = 1000 curve in Fig. 12.11b. Now $\rho_0\lambda = 200 \gg 6$, so the

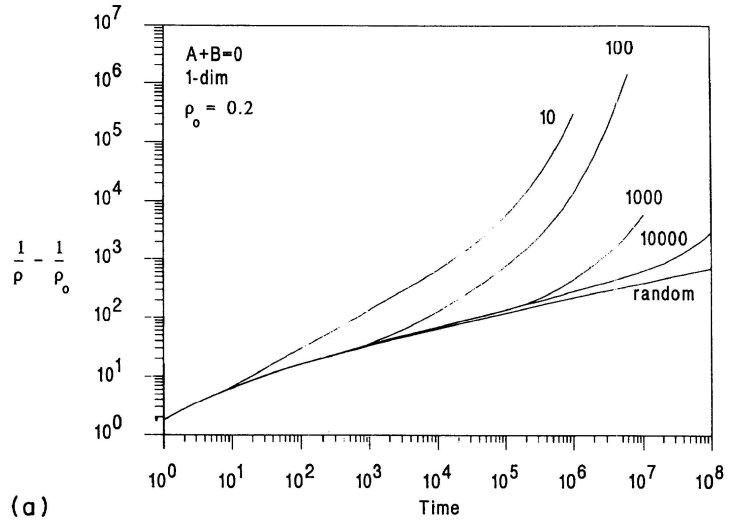

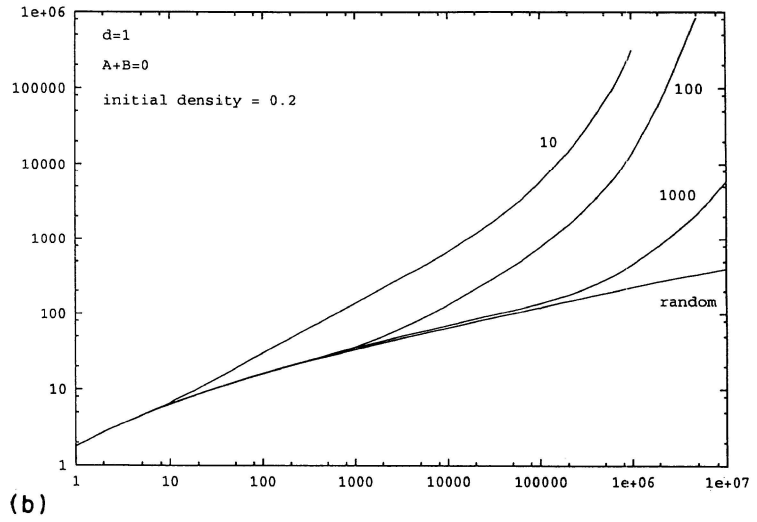

FIGURE 12.11. $\langle\rho\rangle^{-1} - \rho_o^{-1}$ vs. t for one-dimensional lattices of one million sites with various correlation lengths λ, as indicated. The initial density of each species in all cases is $\rho_o = 0.2$. (a) and (b) differ in the time length of the simulations. The "random" curves in both are for a random initial condition and are the same as the L = 1,000,000 curve in Fig. 12.2.

expected kinetic progression is again as shown in Fig. 12.8a. The time $t_s \sim 10^2$ is still well within the regime where the $\lambda = 1000$ curve is essentially the same as the random initial condition curve. The faster decay of the density is expected to set in at $t_c = 2.5 \times 10^5$, which is consistent with the observed behavior. The reactant density predicted from Eq. (12.32) at this onset is $\rho_c \sim 10^{-2}$, which is again consistent with the density obtained from Fig. 12.11b at t_c. The crossover into the slow burst regime is predicted at $t_{sb} \sim 10^6$, only a factor of 5 above t_c. This range is too narrow to extract a reliable slope, even though the curve does go through a slope of 3/4 within the range. A sharp increase beyond the slope of 3/4 is clearly observed in the last decade of the simulation, indicative of the slow burst.

For the $\lambda = 100$ case, with $\rho_0\lambda = 20$, we are still in the kinetic progression of Fig. 12.8a, but some of the kinetic regimes become extremely narrow. The curve hugs the random curve beyond time $t_s \sim 10^2$ and into the Zeldovich regime, but the time $t_c = 2.5 \times 10^3$ is only about an order of magnitude beyond t_s. Therefore, the slope 1/4 is never achieved; instead, the lowest observed slope is 1/3. The time t_{sb} in turn is only about twice t_c. Therefore, the slow burst starts almost immediately beyond t_c. Each simulation for $\lambda = 100$ is ended when only about one particle of each type remains.

When $\lambda = 10$ the kinetic progression is as shown in Fig. 12.10a (with a slow burst). This is the same curve as the $A + B$ curve in Fig. 12.9. Here, the progression goes directly from the $t^{-1/2}$ behavior to the slow burst regime. Again, simulations were ended when only about one particle of each type remained.

Note that a return from the slow burst to an uncorrelated $A + A$ behavior is not observed in any of the cases shown in Fig. 12.11b. Presumably, finite system size effects obfuscate this regime.

In Fig. 12.12 we consider a number of one-dimensional cases that fall within the parameter regimes of "dynamics without segregation," that is, appropriate to the kinetic regimes shown in Fig. 12.10a, both with $\lambda\rho_0 < 1$ and with $\lambda\rho_0 > 1$. The solid curves are the $A + B$ simulations. As a baseline for comparison, we include the curve for a random initial distribution of reactants. This is the same as the $\rho_0 = 0.002$ curve in Fig. 12.4. Here, as in Fig. 12.4, we see that almost the entire curve lies in the $A + A$ depletion zone regime ($t^{-1/2}$), and only in the last time decade in Fig. 12.12 is there a beginning of the crossover into the Zeldovich regime. The time t_s is about 10^6. The dashed line in Fig. 12.12 is the result of $A + A \to 0$ simulations with $\rho_0 = 0.002$ and random initial condition. The $A + A$ and $A + B$ curves are clearly similar until the crossover of the $A + B$ curve begins. The long-time slope of the dashed line is 0.56.

Consider now the finite λ cases, starting with the smallest value of λ. In Fig. 12.12, the solid curve is the $A + B$ simulation, and the diamonds are the results of $A + A \to 0$ simulations. As noted earlier, we expect (and, indeed, see) essentially identical behavior of the two in this tightly correlated situation. Since $\rho_0\lambda = 0.02 \ll 1$, we expect to be squarely within the "fast burst" kinetic progression of Fig. 12.10a. Indeed, at early times the $\lambda = 10$ curve hugs the random initial condition curve. The time $t_c = 25$ is within the range of the observed fairly sharp burst. Once the burst is over, the curve reverts to the expected $t^{-1/2}$ behavior:

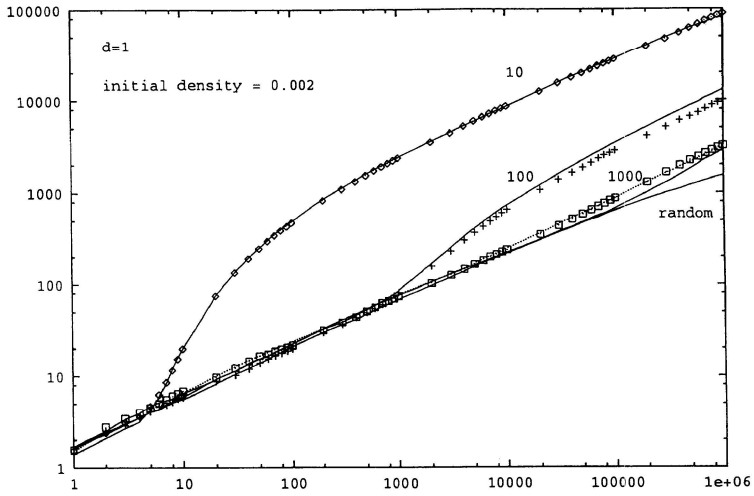

FIGURE 12.12. $\langle \rho \rangle^{-1} - \rho_0^{-1}$ vs. t for one-dimensional lattices of one million sites with various correlation lengths λ, as indicated. The initial density of each species in all cases is $\rho_0 = 0.002$. The solid curves are for the $A + B \rightarrow 0$ simulations. The dashed curve is for simulations of the reaction $A + A \rightarrow 0$ with random initial conditions. The symbols are for $A + A$ simulations with $\lambda = 10$ (diamonds), $\lambda = 100$ (pluses), and $\lambda = 1000$ (squares).

The observed slope is 0.52. Finite system size effects are not reached within this simulation.

When $\lambda = 100$ we are still in the fast burst regime of Fig. 12.10a, since $\rho_0\lambda = 0.2 < 1$. The solid curve for the $A + B$ simulation and the +'s for the $A + A$ simulation are almost the same (the initial correlations are of course not as tight as for $\lambda = 10$). The curve again hugs the random initial condition curve, and the burst crossover time is expected at about $t_c = 2500$. This is again well within the crossover region. Beyond the burst, the slope again reverts to the expected 1/2 (the actual value is 0.53).

When $\lambda = 1000$ we have $\rho_0\lambda = 2$; that is, we now expect a slow burst rather than a fast burst. Note that $\rho_0\lambda$ has the same value as for the curves in Fig. 12.9. The solid curve is the $A + B$ curve, the squares are the simulations for $A + A$ with $\lambda = 1000$, and recall that the dashed curve is for $A + A \rightarrow 0$ with random initial conditions. The three curves are obviously very close. The slow burst is expected to begin at $\sim 2.5 \times 10^5$, and the $A + B$ curve may show an early indication of this effect.

In Fig. 12.13 we show the curves for the $A + B$ reaction in one dimension with $\lambda = 10$ for various initial densities. The $\rho_0 = 0.002$ curve is the same as the $\lambda = 10$ curve in Fig. 12.12, and the $\rho_0 = 0.2$ curve is the same as the $\lambda = 10$ curve

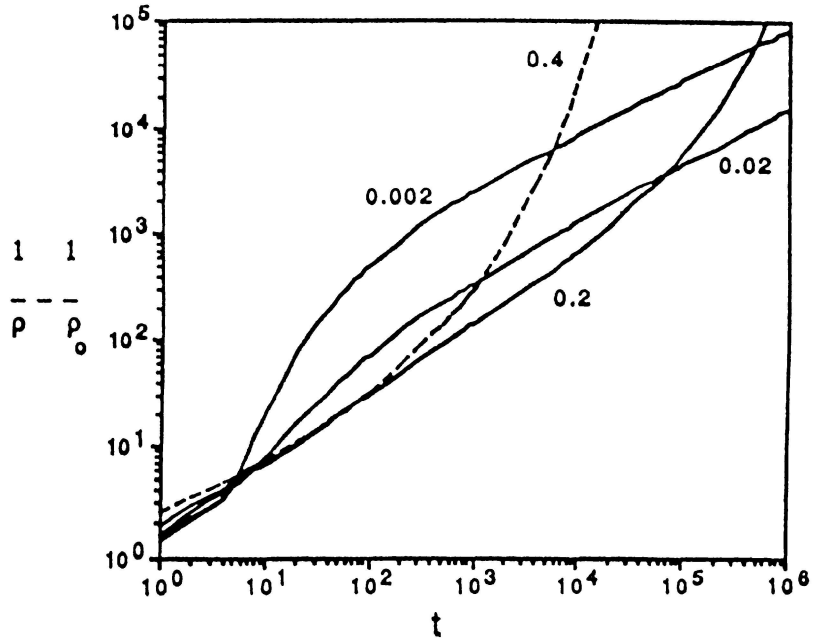

FIGURE 12.13. $\langle\rho\rangle^{-1} - \rho_0^{-1}$ vs. t for different initial densities. In all cases A–B pairs are initially placed $\lambda = 10$ sites apart.

in Fig. 12.11b. Figure 12.13 illustrates the transition from the kinetic progression involving a fast burst to one involving a slow burst. Most notable is the observation that the density curves *cross*; that is, at long times a system with an initially *higher* density has fewer particles left than one with an initial density 10 or even 100 times lower! These crossings must be a consequence of the different particle distributions in the different cases, leading to a rate that is not just dependent on the value of the global density. For the $\rho_0 = 0.02$ and the $\rho_0 = 0.002$ curves, the long time slopes are 1/2 and the interparticle distributions are those characteristic of the $A+A$ depletion zone; that is, a skewed exponential [18]. For the $\rho_0 = 0.2$ curve, we do not know the particle distribution, but it clearly must be different.

Figure 12.14 is similar to Fig. 12.13, but now $\lambda = 100$. The crossover t_c is expected at 2.5×10^3. The $\rho_0 = 0.02$ curve ($\rho_0\lambda = 0.2 < 1$) shows a fast burst in that regime, and the 0.2 and 0.4 curves ($\rho_0\lambda = 20$ and 40) exhibit slow bursts starting about then (note that the 0.2 curve is the same as the $\lambda = 100$ curve in Fig. 12.11b). The $\rho_0 = 0.02$ curve (which, with $\rho_0\lambda = 2$, is in the slow burst regime) marks the transition between the fast burst and slow burst behavior. Note that both the 0.02 and 0.002 curves have slopes of about 1/2 before as well as after the burst.

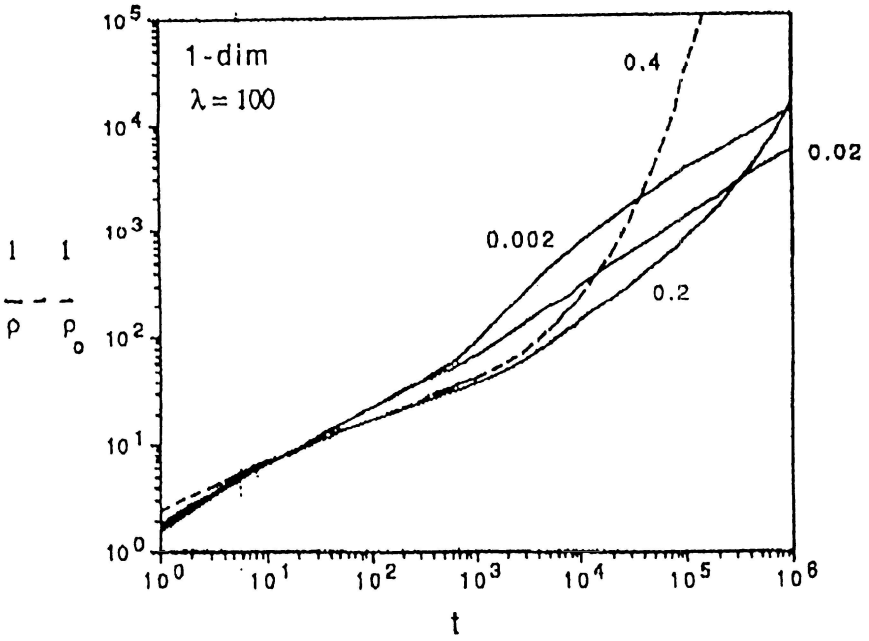

FIGURE 12.14. $\langle\rho\rangle^{-1} - \rho_0^{-1}$ vs. t for different initial densities. In all cases A–B pairs are initially placed $\lambda = 100$ sites apart.

Thus, this figure clearly illustrates the change in behavior from the slow burst that follows the aggregate shrinkage (Fig. 12.8a) through the slow burst in the absence of segregation to the fast burst (Fig. 12.10a) as $\rho_0\lambda$ decreases. For fixed λ we expect the onset of these various bursts to occur at about the same time, $t \sim t_c$, as indeed they do in Fig. 12.14 at around $t \sim 2.5 \times 10^3$.

12.6 Summary

In this final section, we summarize our major results. We do this separately for the random and correlated initial conditions.

For the random initial conditions, we find three main novel features:

1. At early times, the $A+B \rightarrow 0$ system does *not* segregate. Instead, it behaves exactly as does the $A + A \rightarrow 0$ system, with both classical t^{-1} and non-classical $t^{-d/2}$ (for $d \leq 2$) behavior.

2. This behavior stops at a time t_s, when segregation begins. We have found

scaling laws for t_s and for the density ρ_s at time t_s. Our simulations yield the unknown dimension-specific parameters for $d = 1$ and $d = 2$.

3. Eventually, finite system size effects set in at a time t_f whose scaling behavior we have confirmed. Again, we have determined dimension-specific parameters for $d = 1$ and $d = 2$ from our simulations. These results provide information on the segregation process in infinite lattices.

Our simulations are in excellent agreement with our theoretical predictions.

For correlated initial conditions, we have clarified the variety and complexity of different time progressions as a function of the initial conditions. The most important characterizing parameter is the product $\rho_0\lambda^d$ of the initial density and the correlation volume. If this product is small, we find the following principal features:

1. The $A + B \to 0$ reaction behaves exactly as the $A + A \to 0$ reaction for the same values of ρ_0 and λ. In particular, there is no segregation in the $A + B$ system in this case. Neither one of these two reactions has been studied before our work in this regime to the best of our knowledge.

2. At early times, the behavior is that of the uncorrelated $A + A$ problem, again including both classical and nonclassical regimes. At time $t_c = \lambda^2/8D$, an increase (burst) in the reaction rate is observed, which arises from the annihilation of correlated pairs.

3. Once the burst is over, the behavior settles back to the uncorrelated nonclassical $A + A$ form and/or behavior caused by finite system size effects.

When $\rho_0\lambda^d$ is large, segregation does occur in the $A + B \to 0$ reaction. The progression of events is as follows:

1. At early times, the $A + B \to 0$ reaction again (as always) behaves the same as the $A + A \to 0$ reaction (classical, $t^{-d/2}$).

2. The $A + B$ system departs from this behavior at the same time t_s determined in the random initial condition problem, and segregation begins ($t^{-d/4}$).

3. The segregation process is halted at time $t_c = \lambda^2/8D$, when the aggregates, which at this point are of linear size $\sim \lambda$, actually begin to shrink ($t^{-(d+2)/4}$) until only one particle per aggregate remains at time t_{es}.

4. At a time t_{sb}, which is of order $\lambda^2/2D$ beyond t_{es}, there is a (slow) burst when these remaining particles meet. These are not the originally correlated particles, so one might call this a *burst echo* or *delayed burst*.

5. Once the burst has exhausted itself, the nonclassical $A + A$ behavior resumes and/or finite size effects take over.

12.7 Appendix: Solution of Difference Equations

The solution of the linear diffusion equation, Eq. (12.3), is well known to be given by

$$\gamma(\mathbf{r}, t) = \frac{1}{V}\sum_{\mathbf{k}} \int d\mathbf{r}' e^{-i\mathbf{k}\cdot(\mathbf{r}-\mathbf{r}')} e^{-Dk^2 t} \gamma(\mathbf{r}', 0), \tag{12.37}$$

where, for periodic boundary conditions, $\mathbf{k} = 2\pi \boldsymbol{n}/V$ and $\boldsymbol{n}$ is a d-tuple of integers. We need to evaluate the mean square quantity $\langle \gamma^2(\mathbf{r}, t)\rangle$, where the brackets indicate the average over the initial distribution of A's and B's,

$$\langle \gamma^2(\mathbf{r}, t)\rangle = \frac{1}{V^2}\sum_{\mathbf{k}_1}\sum_{\mathbf{k}_2} \int d\mathbf{r}_1 e^{-i\mathbf{k}_1\cdot(\mathbf{r}-\mathbf{r}_1)} \int d\mathbf{r}_2 e^{-i\mathbf{k}_2\cdot(\mathbf{r}-\mathbf{r}_2)} \times e^{-D(k_1^2+k_2^2)t} \langle \gamma(\mathbf{r}_1, 0)\gamma(\mathbf{r}_2, 0)\rangle, \tag{12.38}$$

with Eq. (12.5):

$$\langle \gamma(\mathbf{r}_1, 0)\gamma(\mathbf{r}_2, 0)\rangle = \frac{1}{4}\langle \sum_{j=1}^{N} [\delta(\mathbf{r}_1 - \mathbf{r}_j^A) - \delta(\mathbf{r}_1 - \mathbf{r}_j^B)] \sum_{j=1}^{N} [\delta(\mathbf{r}_2 - \mathbf{r}_j^A) - \delta(\mathbf{r}_2 - \mathbf{r}_j^B)]\rangle. \tag{12.39}$$

Only two distinct types of terms occur in this average. One is of the form $\langle \delta(\mathbf{r}_1 - \mathbf{r}_1^A)\delta(\mathbf{r}_2 - \mathbf{r}_1^B)\rangle$, which for random initial conditions separates into the product of the averages,

$$\langle \delta(\mathbf{r}_1 - \mathbf{r}_1^A)\delta(\mathbf{r}_2 - \mathbf{r}_1^B)\rangle = \langle \delta(\mathbf{r}_1 - \mathbf{r}_1^A)\rangle \langle \delta(\mathbf{r}_2 - \mathbf{r}_1^B)\rangle = \frac{1}{V^2}, \tag{12.40}$$

and for correlated initial conditions is

$$\langle \delta(\mathbf{r}_1 - \mathbf{r}_1^A)\delta(\mathbf{r}_2 - \mathbf{r}_1^B)\rangle = \int d\mathbf{r}_1^A \int d\mathbf{r}_1^B \delta(\mathbf{r}_1 - \mathbf{r}_1^A)\delta(\mathbf{r}_2 - \mathbf{r}_1^B) p(\mathbf{r}_1^A, \mathbf{r}_1^B) = \frac{\Gamma(d/2)}{2V\pi^{d/2}} \int d\Omega \delta(\mathbf{r}_1 - \mathbf{r}_2 - \mathbf{c}). \tag{12.41}$$

The other type of term that appears in Eq. (12.39) is

$$\langle \delta(\mathbf{r}_1 - \mathbf{r}_1^A)\delta(\mathbf{r}_2 - \mathbf{r}_1^A)\rangle = \int d\mathbf{r}_1^A \frac{1}{V}\delta(\mathbf{r}_1 - \mathbf{r}_1^A)\delta(\mathbf{r}_2 - \mathbf{r}_1^A) = \frac{1}{V}\delta(\mathbf{r}_1 - \mathbf{r}_2). \tag{12.42}$$

With proper weighting of these contributions, we find for random initial conditions

$$\langle \gamma(\mathbf{r}_1, 0)\gamma(\mathbf{r}_2, 0)\rangle = -\frac{N}{2V^2} + \frac{N}{2V}\delta(\mathbf{r}_1 - \mathbf{r}_2). \tag{12.43}$$

Substituting this result into Eq. (12.38) readily yields

$$\langle \gamma^2(\mathbf{r}, t)\rangle = -\frac{N}{2V^2} + \frac{N}{2V^2}\sum_{\mathbf{k}_1} e^{-2Dk_1^2 t}. \tag{12.44}$$

With correlated initial conditions

$$\langle \gamma(\mathbf{r}_1,0)\gamma(\mathbf{r}_2,0)\rangle = -\frac{N}{2}\frac{\Gamma(d/2)}{2V\pi^{d/2}}\int d\Omega\delta(\mathbf{r}_1-\mathbf{r}_2-\mathbf{c})+\frac{N}{2}\frac{1}{V}\delta(\mathbf{r}_1-\mathbf{r}_2), \quad (12.45)$$

and consequently,

$$\langle \gamma^2(\mathbf{r},t)\rangle = \frac{N}{2V^2}\sum_{\mathbf{k}} e^{-2Dk^2t} - \frac{N}{2V^2}\frac{\Gamma(d/2)}{2\pi^{d/2}}\sum_{\mathbf{k}}\int d\Omega e^{i\mathbf{k}\cdot\mathbf{c}}e^{-2dk^2t}. \quad (12.46)$$

The sums in Eqs. (12.44) and (12.45) cannot in general be done in closed form except in the large-volume limit, where they can be converted to integrals according to

$$\lim_{V\to\infty}\frac{1}{V}\sum_{\mathbf{k}} f(\mathbf{k}) = \frac{1}{(2\pi)^d}\int d\mathbf{k} f(\mathbf{k}). \quad (12.47)$$

The resulting integrals can easily be carried out to yield Eqs. (12.10) and (12.11).

12.8 Appendix: Initial Averages

It is useful to first deal with initial averages for a discrete system in which the A and B molecules occupy lattice sites separated by lattice constant a. Subsequently, we discuss the continuum limit. Molecules A and B are initially located at sites $\boldsymbol{l}_j^A$ and $\boldsymbol{l}_j^B$, respectively, with $j = 1, 2, \ldots, N$. In place of $p(\mathbf{r}^A)d\mathbf{r}^A$ and $p(\mathbf{r}^B)d\mathbf{r}^B$ of Eq. (12.7), we now have $p(\boldsymbol{l}^A) = p(\boldsymbol{l}^B) = 1/L$. The average initial density of A molecules is

$$\langle \rho_A^{\text{lat}}(\boldsymbol{l},0)\rangle = \sum_{\{\boldsymbol{l}_j^A\}} \rho_A^{\text{lat}}(\boldsymbol{l},0)\prod_{j=1}^{N} p(\boldsymbol{l}_j^A), \quad (12.48)$$

where in analogy with Eq. (12.5) we have

$$\rho_A^{\text{lat}}(\boldsymbol{l},0) = \sum_{j=1}^{N}\delta(\boldsymbol{l},\boldsymbol{l}_j^A), \quad (12.49)$$

and δ is the Kronecker delta. We readily find that $\langle \rho_A^{\text{lat}}(\boldsymbol{l},0)\rangle = \langle \rho_B^{\text{lat}}(\boldsymbol{l},0)\rangle = N/L$, as must be the case. The average of the square of the initial density of A particles is also readily calculated, and one finds

$$\langle [\rho_A^{\text{lat}}(\boldsymbol{l},0)]^2\rangle = \frac{N(N-1)}{L^2} + \frac{N}{L}. \quad (12.50)$$

Note that $\langle [\rho_A^{\text{lat}}(\boldsymbol{l},0)]^2\rangle \neq \langle \rho_A^{\text{lat}}(\boldsymbol{l},0)\rangle^2$ and that in fact the difference between them is *larger* than $\langle \rho_A^{\text{lat}}\rangle^2$ when $N/L < 1$.

The average of the product of the initial densities of A's and B's for random initial conditions is the product of the averages, $\langle \rho_A^{\text{lat}}(\boldsymbol{l},0)\rho_B^{\text{lat}}(\boldsymbol{l},0)\rangle = N^2/L^2$.

For correlated initial conditions, we set $c = a\lambda$, where λ is an integer. In one dimension, the discrete version of the probability density in Eq. (12.9) simply places the B partner of an A molecule at either of the lattice sites λ or $-\lambda$ units from A with equal probability. In higher dimensions, a problem immediately arises of how to formulate a discrete version of the continuum probability density in Eq. (12.9). A simple (not necessarily optimal) procedure in two dimensions is to place the B partner of a given A molecule either north, south, east, or west of it with equal probability. The discrete form replacing Eq. (12.9) then is

$$p(\boldsymbol{l}^A, \boldsymbol{l}^B) = \frac{1}{2dL} \sum_{\boldsymbol{m}} \delta(\boldsymbol{l}^A - \boldsymbol{l}^B, \boldsymbol{m}), \tag{12.51}$$

where in one dimension $\boldsymbol{m} = \lambda$ and $\boldsymbol{m} = -\lambda$; in two dimensions $\boldsymbol{m} = (\lambda, 0)$, $(-\lambda, 0)$, $(0, \lambda)$, and $(0, -\lambda)$. The average of the product of the initial densities of A and B molecules now is

$$\langle \rho_A^{\text{lat}}(\boldsymbol{l}, 0)\rho_B^{\text{lat}}(\boldsymbol{l}, 0)\rangle = \sum_{\{\boldsymbol{l}_j^A\}} \sum_{\{\boldsymbol{l}_j^B\}} \rho_A^{\text{lat}}(\boldsymbol{l}, 0)\rho_B^{\text{lat}}(\boldsymbol{l}, 0) \prod_{j=1}^{N} p(\boldsymbol{l}_j^A, \boldsymbol{l}_j^B)$$

$$= \frac{N(N-1)}{L^2} \qquad \text{if } \lambda \neq 0, \tag{12.52}$$

$$= \frac{N(N-1)}{L^2} + \frac{N}{L} \qquad \text{if } \lambda = 0, \tag{12.53}$$

independent of dimensionality. Thus, unless the A–B pair lands on exactly the same site, the average of the product reduces to the product of the averages as in the random initial condition case (except for the small difference N/L^2). In our simulations $\lambda = 0$ is not allowed.

The continuum version of the average density in Eq. (12.48) is

$$\langle \rho_A(\mathbf{r}, 0)\rangle = \int \cdots \int \prod_{j=1}^{N} d\mathbf{r}_j^A \rho_A(\mathbf{r}, 0) \prod_{j=1}^{N} p(\mathbf{r}_j^A)., \tag{12.54}$$

and one straightforwardly finds $\langle \rho_A(\mathbf{r}, 0)\rangle = \langle \rho_B(\mathbf{r}, 0)\rangle = N/V$. The correspondence between the discrete and continuum mean square densities is somewhat more problematic. Dividing Eq. (12.50) by a^{2d} yields

$$\langle \rho_A^2(\mathbf{r}, 0)\rangle = \frac{N(N-1)}{V^2} + \frac{N}{V}\frac{1}{a^d}. \tag{12.55}$$

The second term clearly diverges as $a \to 0$. Indeed, a calculation based directly on the continuum average yields

$$\langle \rho_A^2(\mathbf{r}, 0)\rangle = \frac{N(N-1)}{V^2} + \frac{N}{V} \int d\mathbf{r}^A [\delta(\mathbf{r} - \mathbf{r}^A)]^2, \tag{12.56}$$

where the second term, being an integral of the square of a δ function, clearly diverges. Equation (12.55) provides insight into the nature of this divergence.

The calculation of $\langle \rho_A(\mathbf{r},0)\rho_B(\mathbf{r},0)\rangle$ for random initial conditions straightforwardly yields, as expected, $\langle \rho_A(\mathbf{r},0)\rho_B(\mathbf{r},0)\rangle = N^2/V^2$. With correlated initial conditions, a transcription of Eqs. (12.52) and (12.53) into the continuum by dividing by a^{2d} gives

$$\langle \rho_A(\mathbf{r},0)\rho_B(\mathbf{r},0)\rangle = \frac{N(N-1)}{V^2} \qquad if \ \ \lambda \neq 0 \tag{12.57}$$

$$= \frac{N(N-1)}{V^2} + \frac{N}{V}\frac{1}{a^d} \quad if \ \ \lambda = 0. \tag{12.58}$$

Note that $\lambda = 0$ corresponds to a vanishing distance c between correlated molecules, and that this in turn means that $c < a$. If in fact the continuum average is carried out explicitly, we obtain the form that embodies the $a \to 0$ result:

$$\langle \rho_A(\mathbf{r},0)\rho_B(\mathbf{r},0)\rangle = \frac{N(N-1)}{V^2} + \frac{N}{V}\frac{\Gamma(d/2)}{2\pi^{d/2}}\int d\Omega\delta(\mathbf{c}). \tag{12.59}$$

12.9 Acknowledgments

We gratefully acknowledge support from the U.S. Department of Energy, grant No. DE-FG03-86ER13606 (K.L.), from the National Science Foundation, grant No. DMR-911622 (R.K.), and from NATO grant No. CRG 920029 (P.A.).

12.10 References

[1] R. Kopelman, *Science* **241**, 1620 (1988).

[2] D. Toussaint and F. Wilczek, *J. Chem. Phys.* **78**, 2642 (1983).

[3] P. Klymko and R. Kopelman, *J. Phys. Chem.* **86**, 3686 (1982).

[4] P. Klymko and R. Kopelman, *J. Phys. Chem.* **87**, 4565 (1983).

[5] D.C. Torney and H.M. McConnell, *J. Phys. Chem.* **87**, 1441 (1983).

[6] R. Kopelman, *J. Stat. Phys.* **42**, 185 (1986).

[7] L.W. Anacker and R. Kopelman, *J. Chem. Phys.* **81**, 6402, (1984).

[8] L.W. Anacker, R.P. Parson, and R. Kopelman, *J. Phys. Chem.* **89**, 4758 (1985).

[9] P. Evesque and J. Duran, *J. Chem. Phys.* **80**, 3016 (1984).

[10] P.W. Klymko and R. Kopelman, *J. Phys. Chem.* **87**, 4565 (1983).

[11] R. Kopelman, S.K. Parus, and J. Prasad, *Chem. Phys.* **128**, 209 (1988).

[12] S. Chandrasekhar, *Rev. Mod. Phys.* **15**, 1 (1943).

[13] K. Lindenberg, B.J. West, and R. Kopelman, *Phys. Rev. A* **42**, 890 (1990).

[14] P. Argyrakis, R. Kopelman, and K. Lindenberg, *Chem. Phys.* **177**, 693 (1993).

[15] K. Lindenberg, P. Argyrakis, and R. Kopelman, *J. Phys. Chem.* **98**, 3389 (1994).

[16] K. Lindenberg, B.J. West, and R. Kopelman, in *Noise and Chaos in Nonlinear Dynamical Systems*, edited by S. Capelin and F. Moss (Cambridge University Press, Cambridge, 1989). See also references therein.

[17] K. Lindenberg, B.J. West, and R. Kopelman, *Phys. Rev. Lett.* **60**, 1777 (1988).

[18] P. Argyrakis and R. Kopelman, *Phys. Rev. A* **41**, 2114, 2121 (1990).

[19] P. Argyrakis and R. Kopelman, *Phys. Rev. A* **45**, 5814 (1992).

[20] P. Argyrakis, *Comp. Phys.* **6**, 525 (1992).

[21] C.R. Doering and D. Ben-Avraham, *Phys. Rev. A* **38**, 3035 (1988).

[22] P. Argyrakis and R. Kopelman, *J. Phys. Chem.* **93**, 225 (1989).

[23] R. Schoonover, D. Ben-Avraham, S. Havlin, R. Kopelman, and G.H. Weiss, *Physica A* **171**, 232 (1991). See also references therein.

[24] F. Leyvraz and S. Redner, *Phys. Rev. Lett.* **66**, 2168 (1991).

[25] F. Leyvraz and S. Redner, *Phys. Rev. A* **46**, 3132 (1992).

[26] D.C. Torney and H.M. McConnell, *Proc. R. Soc. London, Ser. A* **387**, 147 (1983).

[27] R. Kopelman and P. Argyrakis, *J. Chem. Phys.* **72**, 3053 (1980).

[28] P.A. Alemany, D.H. Zanette, and H.S. Wio, *Phys. Rev. E* **50**, 3646 (1994).

[29] V. Kuzovkov and E. Kotomin, *Rep. Prog. Phys.* **51**, 1479 (1988). See also references therein.

[30] A.A. Ovchinnikov and Y.G. Zeldovich, *Chem. Phys.* **B28**, 215 (1978).

[31] K. Kang and S. Redner, *Phys. Rev. Lett.* **52**, 955 (1984).